Reduced-FOV Diffusion Imaging with ZOnal Oblique Multislice (ZOOM) combined with Readout-Segmented (RS)-EPI

S. J. Holdsworth[1], S. Skare[1], R. L. O'Hallaran[1], and R. Bammer[1]
[1]Radiology, Stanford University, Palo Alto, CA, United States

Introduction: Diffusion-weighted imaging (DWI) using echo-planar imaging (EPI) has been limited by geometric distortion and blurring, particularly in regions with large off-resonance effects such as in the spinal-cord and in regions of the brain residing near tissue/air interfaces. Geometric distortion in EPI is proportional to the FOV in the phase encoding direction (FOV_{pe}), as well as the echo-spacing between adjacent echoes in the EPI train (T_{ro}). Parallel imaging, which is frequently used for distortion reduction in EPI scans, is difficult to use for certain geometric arrangements of coils (such as some spine array coils) and for small FOVs (such as in orbital scans). To reduce FOV_{pe} and avoid aliasing, saturation pulses can be used, however the suppression efficiency is generally limited leading to partial aliasing. Spatially selective RF pulses [1,2] can be used, but have limitations in the number of slices that can be prescribed. The zonal oblique multislice EPI (ZOOM-EPI) technique [3-5] is another approach, which uses a tilted refocusing pulse as shown in Fig. 1. To reduce distortion further, T_{ro} can be reduced by covering *k*-space with a series of consecutive segments or 'blinds', known as RS-EPI [6,7] (Fig. 2c). In this work, we implement both the ZOOM pulse together with the RS-EPI trajectory (ZOOM-RSEPI) to get the benefits of both methods for reducing distortion. Fig. 2 illustrates the theoretical reduction in distortion as one goes from a full FOV EPI, to ZOOM-EPI, and finally to ZOOM-RSEPI.

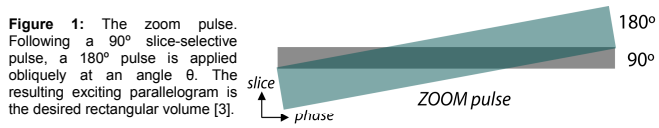

Figure 1: The zoom pulse. Following a 90° slice-selective pulse, a 180° pulse is applied obliquely at an angle θ. The resulting exciting parallelogram is the desired rectangular volume [3].

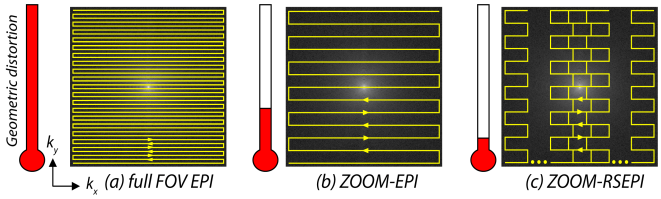

Figure 2: Reduction of distortion as one moves from (a) full-FOV EPI to (b) a rectangular FOV with EPI (zoom-EPI), and (c) a rectangular FOV with RS-EPI (ZOOM-RSEPI). For the parameters used in this work, this 'distortion meter' accompanying the trajectories is drawn to scale.

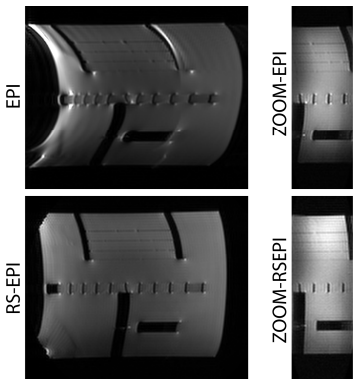

Figure 3: Single-shot EPI and single-shot RS-EPI images (b = 0s/mm^2) acquired on a phantom using using: *(Left column)* a full FOV of 26 cm and matrix size = 180 x 180; *(Right column)* a rectangular FOV = 26 x 7.8 cm and matrix size = 180 x 54 (square pixels).

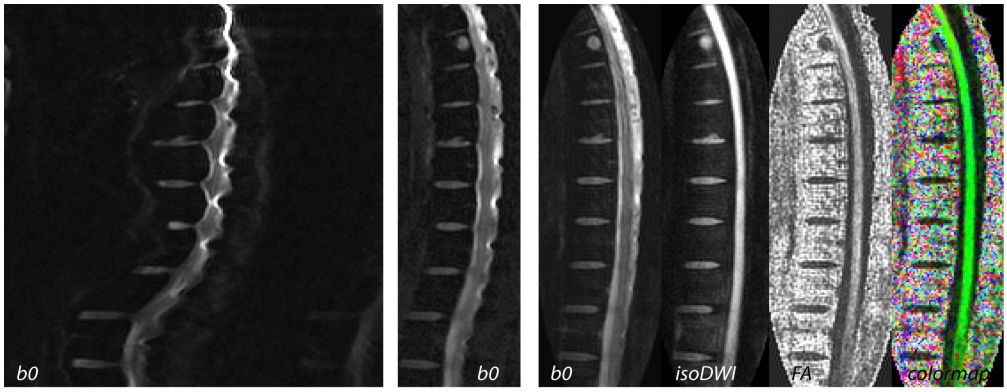

Figure 4: Comparison between the b = 0 s/mm^2 images of a thoracic spine using full FOV EPI (30 x 30 cm, matrix size = 200 x 200), ZOOM-EPI and ZOOM-RSEPI (30 x 10 cm, matrix size = 200 x 60 (square pixels)). For ZOOM-RSEPI, the isotropic DWI (isoDWI, b = 500 s/mm^2), fractional anisotropy (FA), and 1st eigenvector (colormap) are also shown. Note that there is less 'disc bulging' into the spinal canal and less blurring on the ZOOM-RSEPI scans than on the ZOOM-EPI scans.

Methods: All diffusion images were acquired on a 3T whole-body GE DVMR750 system. ZOOM-EPI and ZOOM-RSEPI DW images were first acquired on a phantom (8-channel head coil, single-shot, FOV = 26cm x 7.8cm, matrix size = 180 x 54 (square pixels)). Second, thoracic spine DTI images were acquired on a volunteer using a 4-channel spine coil, followed by a scan of the orbits using a single-channel birdcage coil. The following common parameters were used: rectangular FOV = 30 x 10cm, Δz = 4 mm (zoom-angle θ = 5°, slthck$_{90°}$ = 4mm, slthck$_{180°}$ = 8mm), TR = 3s, a matrix size = 200 x 60 (square pixels), partial Fourier (18 overscans), 24 isotropically distributed DW directions with b = 500 s/mm^2, and a scan time of 9:48mins. ZOOM-RSEPI used TE$_{min}$ = 55 ms, 7 blinds of width = 32 and ZOOM-EPI used TE$_{min}$ = 75 ms, and 7 NEX. For comparison, full FOV images were acquired on the phantom and volunteer. For the orbital scan, the parameters as above were used with Δz = 5 mm, b = 600 s/mm^2, 60 diffusion directions and 4 b = 0 (ZOOM-EPI), 8 diffusion directions with 1 b = 0 (ZOOM-RSEPI), and a scan time of 3:12min.

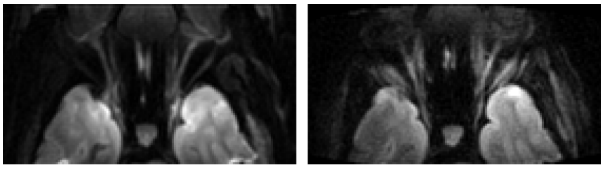

Figure 5: Orbital isoDWI images (b = 600 s/mm^2) acquired using ZOOM-EPI (60 diffusion directions) and ZOOM-RSEPI (8 diffusion directions, 7 blinds), both in a scan time of 3:12min.

Results: The EPI and RS-EPI b = 0 s/mm^2 phantom images acquired with and without the use of rectangular FOV and ZOOM pulse is shown in Fig. 3. As shown, geometric distortion can be reduced significantly with ZOOM-RSEPI. This method also reduces the 'jagged' appearance of the spinal cord as shown in the b = 0 s/mm^2 images (Fig. 4). Fig. 5 compares a ZOOM-EPI and ZOOM-RSEPI scan of the orbits. The eyes, the optic nerve, and the ocular muscles show reduced distortion with ZOOM-RSEPI.

Discussion: This work shows that RS-EPI in combination with the ZOOM pulse in order to spatially select a region of interest may be useful for diffusion imaging of regions with large off-resonance effects. While the rectangular FOV used in this work (30cm x 10cm) reduced distortion by 30% (compared to a full FOV acquisition), RS-EPI further reduced the distortion by 33%. A disadvantage of RS-EPI is the reduced SNR efficiency compared with EPI. However the resulting RS-EPI DTI data shown in Fig. 4 shows high SNR 3T images acquired in a reasonable scan time for DTI, and the jagged appearance that often hampers the quality of EPI DW images is reduced significantly. The orbital scan in Fig. 5 more accurately depicts the shape of the optical nerve, thus may be a useful method for DTI or fiber-tracking of the optical nerve for the early diagnosis of pathology such as multiple sclerosis.

References: [1] Kiefer C. ESMRMB 1999;302 [2] Saritas E. MRM 2008;60:468. [3] Mansfield P. Phys. E: Sci. Instrum. 1988 21:275. [4] Symms M. ISMRM 2000;160. [5] Wheeler-Kingshott, MRM 2002 47:24 [6] Porter D. ISMRM 2004;442. [7] Holdsworth S. ISMRM 2009:6247. **Acknowledgements:** This work was supported in part by the NIH (1R01 EB008706, 1R01 EB008706S1, 5R01 EB002711, 1R01 EB006526, 1R21 EB006860), the Center of Advanced MR Technology at Stanford (P41RR09784), Lucas Foundation, Oak Foundation, and the Swedish Research Council (K2007-53P-20322-01-4).